Journal of Nuclear Materials 450 (2014) 69–74

Contents lists available at SciVerse ScienceDirect

Journal of Nuclear Materials

journal homepage: www.elsevier.com/locate/jnucmat

Characterization of ODS-tungsten microwave-sintered from sol–gel prepared nano-powders

R. Liu, X.P. Wang, T. Hao, C.S. Liu, Q.F. Fang *

Key Laboratory of Materials Physics, Institute of Solid State Physics, Chinese Academy of Sciences, Hefei 230031, China

ARTICLE INFO

Article history:
Available online 4 June 2013

ABSTRACT

Nano-sized W–1%La_2O_3 and W–1%Y_2O_3 powders were synthesized by sol–gel method followed by hydrogen reduction. The average particle size of the powders is smaller than 50 nm. Microwave sintering method was used for the consolidation of tungsten samples, and a relatively low sintering temperature (1500 °C) and short soaking time (30 min) were used to reduce the grains growth. Nano-sized oxide particles with a size distribution of 10–50 nm were homogeneously dispersed in the tungsten matrix. The relative density, average grain size and Vickers micro-hardness of the microwave-sintered W–1%La_2O_3 and W–1%Y_2O_3 samples are 92.4% and 93.6%, 1.1 and 0.7 μm, 6.03 and 4.12 GPa, respectively. The W–1%Y_2O_3 samples showed better sinterability, finer grains, and higher hardness than the W–1%La_2O_3 samples.

1. Introduction

Tungsten is considered as one of the most promising candidates for plasma facing materials in fusion reactors and for spallation neutron source target applications [1–5]. However, tungsten exhibits serious embrittlement in several aspects, i.e., low-temperature brittleness, recrystallization brittleness and irradiation induced brittleness [5–7]. Recently, nano-structured materials have attracted intense interest. It was reported that ultrafine-grained tungsten produced by severe plastic deformation shows reduced brittleness and improved toughness [7–9]. Besides, the anti-irradiation ability of a material is determined by how well the microstructure can remove vacancies and interstitial defects in equal numbers [10]. The large amount of grain boundaries or interfaces in nano-structured materials may act as sinks for irradiation induced point defects, which would improve the irradiation tolerance of materials. Therefore, irradiation embrittlement might be alleviated by decreasing the grain size [11–14]. However, nano-structured metals are generally unstable and their grains grow rapidly even at low temperatures, making them difficult to fabricate and often unsuitable for usage [15]. Due to the high melting temperature, most tungsten based materials are produced by powder metallurgy method. The high temperature and long holding time necessary for the densification of tungsten will result in significant grain growth. Under the high temperatures in sintering or usage process, the mechanical properties and irradiation resistance of nano-structured tungsten would be degraded with the grain coarsening.

Fine grained but thermally stable oxides dispersion strengthened (ODS) tungsten materials have shown improved high temperature strength, creep resistance and recrystallization temperature, as the oxides dispersed in tungsten could inhibit the grain boundary sliding [16–23]. The addition of oxides is an effective method to improve the high temperature stability of nano-structured W materials. Besides, the interfaces between the oxide nano-particles and tungsten matrix may also provide sinks for irradiation induced point defects and contribute to the improvement of the irradiation resistance of materials.

Conventional sintering of tungsten is commonly carried out at temperatures as high as 2000–2500 °C for a long soaking time to achieve full densification [22]. When exposed to high sintering temperature for long time, tungsten nano-particles usually grow rapidly to reduce the high surface energy despite of the restriction of grain movement by oxide particles [16,18]. To obtain fine-grained tungsten materials, it is essential to reduce the sintering temperature and soaking time. Microwave sintering is a relatively new technique, which has been utilized in the consolidation of ceramics and powdered metals including refractory metals and their carbides [24–28]. In the microwave sintering process, the powdered samples absorb microwave energy and heat themselves from the very interior. Therefore, microwave sintering provides several advantages, such as rapid heating rate and short sintering time [24,26], which are beneficial to inhibiting the grain growth.

For the fabrication of ODS-W, mechanical milling is a common method to mix powders and decrease the particle size. In one of our previous works fine grained ODS-W was fabricated using mechanical milling and microwave sintering method [29]. Nevertheless, the homogeneity of powders is limited by the initial powders and milling condition. In the current work, sol–gel method

* Corresponding author. Tel.: +86 551 5591459; fax: +86 551 5591434.
E-mail address: qffang@issp.ac.cn (Q.F. Fang).

0022-3115/$ - see front matter © 2013 Elsevier B.V. All rights reserved.
http://dx.doi.org/10.1016/j.jnucmat.2013.05.049

combined with hydrogen reduction was used for the synthesis of tungsten nano-powders. As the dissolved precursor materials are mixed at molecular level, it is expected that oxides can be dispersed with higher homogeneity. The microstructures of sol–gel synthesized tungsten nano-powders and microwave-sintered ODS-W samples were characterized. The effects of La_2O_3 and Y_2O_3 nano-particles on the consolidation behavior, microstructure and mechanical properties of tungsten were investigated.

2. Experimental details

Oxide dispersion strengthened (ODS) tungsten with compositions of W–1 wt%La_2O_3 and W–1 wt%Y_2O_3 were synthesized. At first, citric acid ($C_6H_8O_7{\cdot}H_2O$) was dissolved in deionized water, and then lanthanum nitrate hydrate, $La(NO_3)_3{\cdot}6H_2O$ or yttrium nitrate hydrate, $Y(NO_3)_3{\cdot}6H_2O$ and ammonium paratungstate, $(NH_4)_{10}[H_2W_{12}O_{42}]{\cdot}4H_2O$ were added into the solution. After 2 h stirring at 80 °C, a small amount of polyethylene glycol (PEG, Molecular weight 20,000) were added into the solution. The solution was heated at 80 °C with stirring until a gel formed. The obtained gel was heated at 120 °C for 10 h to remove water and then was calcined at 550 °C for 6 h in air to remove the organic materials. After calcination, a light-yellow mixture of tungsten oxides and lanthanum (or yttrium) oxides were obtained. The oxides mixture was then reduced at 780 °C for 2 h in flowing hydrogen, resulting in oxide doped tungsten powders.

The sol–gel synthesized tungsten powders were pressed into a cylindrical mold at 400 MPa in air without any binders. The green compacts are 13 mm in diameter and about 3 mm in height. Microwave sintering was carried out in a multimode microwave furnace (HAMiLab-V3000, Changsha Syno-therm Co., Ltd., China) with a 0.3–3 kW microwave generator operated at 2.45 GHz. Temperature was monitored by an infrared pyrometer (Raytek RAYMM2MHSF1L) installed at the top of the vacuum chamber. The ODS-W samples were microwave-sintered at 1500 °C with a soaking time of 30 min. The heating rate was controlled as 25 °C/min bellow 1000 °C. The temperature profile of microwave-sintering process was described in detail elsewhere [29]. All samples in this study were microwave-sintered following the same sintering program.

Chemical analysis was carried out to determine the C, N, O contents in microwave-sintered tungsten. Inductively coupled plasma atomic emission spectroscopy (ICP-AES) was used to analyze the La and Y content. The density of sintered samples was determined by Archimedes principle. The theoretical density of the ODS-W composites was calculated from the fraction and theoretical density of each component. The theoretical density of tungsten, La_2O_3 and Y_2O_3 was adopted as 19.3, 6.51 and 5.01 g/cm^3, respectively. X-ray diffractometer (Philips X'pert PRO).) was used to study the phases of sol–gel prepared oxides precursors and hydrogen reduced powders. Microstructure of sol–gel synthesized powders and microwave-sintered samples were characterized with a field-emission scanning electron microscopy (FESEM, Sirion 200, FEI) and a transmission electron microscope (TEM, JEM-2000FX). Energy dispersive X-ray (EDX, INCA) analytical system installed on TEM was used for elemental analysis. Polished ODS-W samples were subjected to Vickers micro-hardness testing at room temperature with a load of 100 g and a dwell time of 10 s.

3. Results and discussion

Sol–gel produced oxides precursors and hydrogen reduced powders were analyzed by XRD. As an example, Fig. 1a shows the XRD patterns of precursor oxides of W–1%Y_2O_3 sample calcinated at 550 °C for 6 h. The XRD peaks of WO_3 were observed,

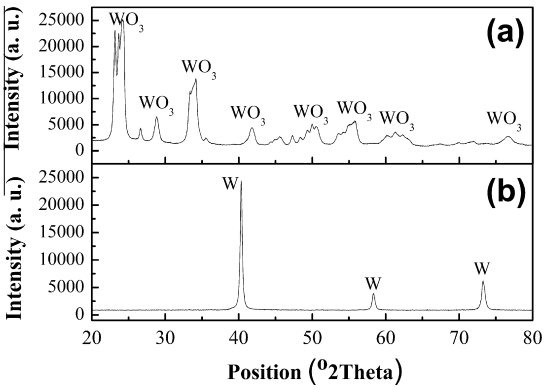

Fig. 1. XRD patterns of (a) sol–gel produced tungsten and yttrium oxides calcined at 550 °C for 6 h and (b) W–1%Y_2O_3 powders after 2 h hydrogen reduction at 780 °C.

however, no yttrium oxides peaks were found due to the small amount. Fig. 1b shows the XRD patterns of W–1%Y_2O_3 powders reduced at 780 °C for 2 h in flowing hydrogen. Only the diffraction peaks of bcc tungsten were detected, which indicates that the tungsten oxides have been completely reduced into tungsten. However, the Y_2O_3 phase would be stable under this reducing conditions, and were not detected owing to the small amount of only 1 wt%.

The SEM micrographs of sol–gel synthesized oxides-doped tungsten powders are presented in Fig. 2. As shown in Fig. 2, the particle sizes of W–1%La_2O_3 (Fig. 2a) and W–1%Y_2O_3 (Fig. 2b) powders are all nano-sized, and a little aggregation was found in the W–1%Y_2O_3 powders. However, due to the small size of the sol–gel produced tungsten powders, it is difficult to accurately determine the particle size from the SEM micrographs.

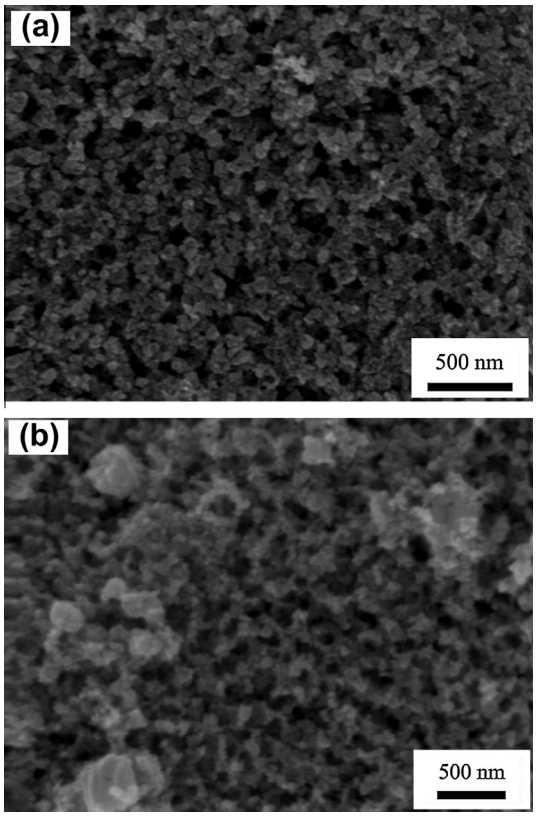

Fig. 2. SEM micrographs of sol–gel synthesized powders (a) W–1%La_2O_3 and (b) W–1%Y_2O_3, after 2 h hydrogen reduction at 780 °C.

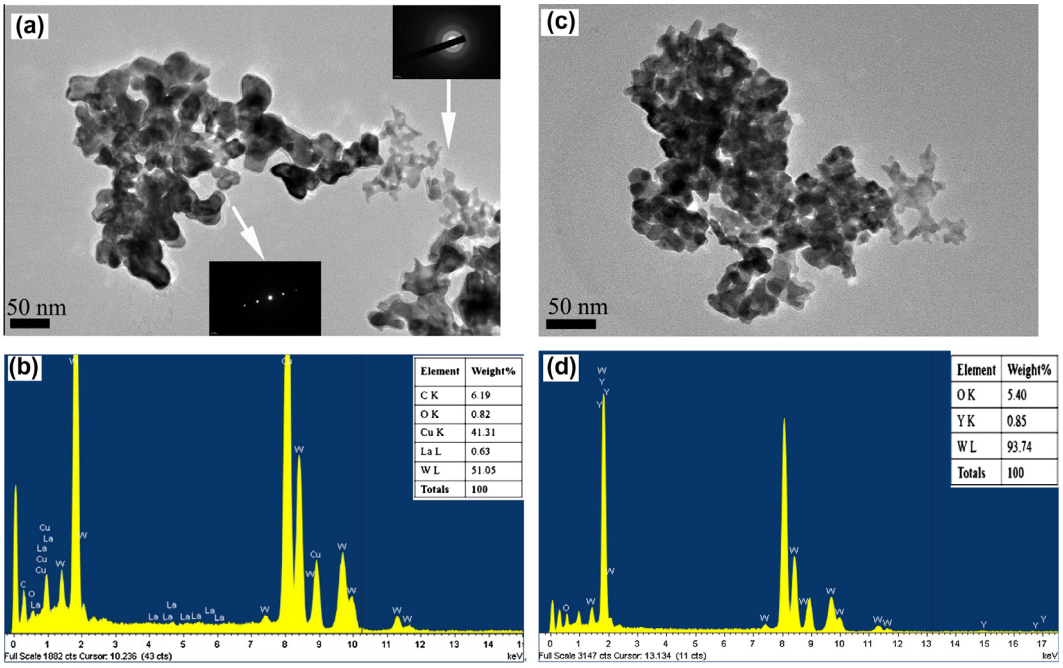

Fig. 3. TEM images of sol–gel synthesized W–1%La_2O_3 powders (a) and its corresponding EDX pattern (b), and TEM images of W–1%Y_2O_3 powders (c) and its EDX pattern (d).

To further characterize the microstructure of sol–gel synthesized tungsten powders, the oxides doped tungsten powders were ultrasonically dispersed in anhydrous ethanol and then subjected to TEM analysis. Fig. 3a and c shows the TEM micrographs of W–1%La_2O_3 and W–1%Y_2O_3, respectively. The size of tungsten particles is in the range from 10 to 50 nm. The insets in Fig. 3a are the electron diffraction patterns taken from tungsten particles and oxide particles. The results suggest that tungsten particles are well crystallized, while the oxides exhibit a typical amorphous structure. The EDX results were also shown for sol–gel produced W–1%La_2O_3 (Fig. 3b) and W–1%Y_2O_3 (Fig. 3d) powders. Oxygen and lanthanum or yttrium signals were detected and the content of lanthanum or yttrium is close to the designed value (1 wt% La_2O_3 or Y_2O_3). The exact contents of La and Y in microwave-sintered samples were determined by inductively coupled plasma atomic emission spectroscopy (ICP-AES), as listed in Table 1. Besides, the C, N, O contents given by chemical analysis were also list in Table 1. The Y content is 0.80%, which is close to the theoretical value (0.79 wt%). The La content is 0.86%, showing well consist with the theoretical value (0.85 wt%). The results indicate that the contents of tungsten composites can be easily controlled through sol–gel method.

The relative density of microwave-sintered W–1 wt%La_2O_3 and W–1 wt%Y_2O_3 by sol–gel method is 92.4% and 93.8%, respectively, as listed in Table 2, where the average grain size and Vickers micro-hardness of microwave-sintered ODS-W from sol–gel synthesized powders were also given and the results of microwave-sintered ODS-W from ball-milled commercial powders were also listed for comparison [29]. In comparison with the ODS-W samples from ball-milled commercial powders, the relative density of W–1 wt%La_2O_3 and W–1wt%Y_2O_3 samples from sol–gel synthesized powders showed lower values. One possible reason is the higher porosity of green compacts due to the aggregation of sol–gel produced nano-powders. As the ball-milling process could alleviate the aggregation of powders, compacts from the ball-milled powders showed much higher initial density (about 56%) than that from sol–gel produced powders (about 42%). Besides, as the oxides could inhibit the movement of grain boundaries and influence the consolidation process, more homogeneous oxides dispersion in sol–gel synthesized tungsten samples may also lead to lower relative density. To achieve higher relative density improvement of the sintering procedure and post thermo-mechanical treatment must be applied.

For both sol–gel and ball-milling methods, W–1%Y_2O_3 exhibits higher density than W–1%La_2O_3. Kim et al. [16] have also found that the W–Y_2O_3 system has the highest sinterability among the W–Y_2O_3, W–HfO_2, and W–La_2O_3 systems when they were sintered by spark plasma sintering method.

Table 1
Chemical compositions of microwave-sintered tungsten samples.

Materials	C (%)	N (%)	O (%)	La (%)	Y (%)
W–1 wt%La_2O_3	0.20	0.0050	0.27	0.86	–
W–1 wt%Y_2O_3	0.26	0.0053	0.30	–	0.80

Table 2
Main results of tungsten materials fabricated by sol–gel method and mechanical ball-milling method, microwave-sintered at 1500 °C for 30 min.

Materials	Method	Density (g/cm^3)	Relative density (%)	Grain size (μm)	H_{V100g} (GPa)
W–1 wt%La_2O_3	Sol–gel	17.49	92.4	1.1	4.12 ± 0.25
W–1 wt%Y_2O_3	Sol–gel	17.60	93.8	0.7	6.03 ± 0.25
W–1 wt%La_2O_3	Ball-milling	18.0	95.0	1.4	4.21 ± 0.25
W–1 wt%Y_2O_3	Ball-milling	18.2	96.8	0.7	6.91 ± 0.20

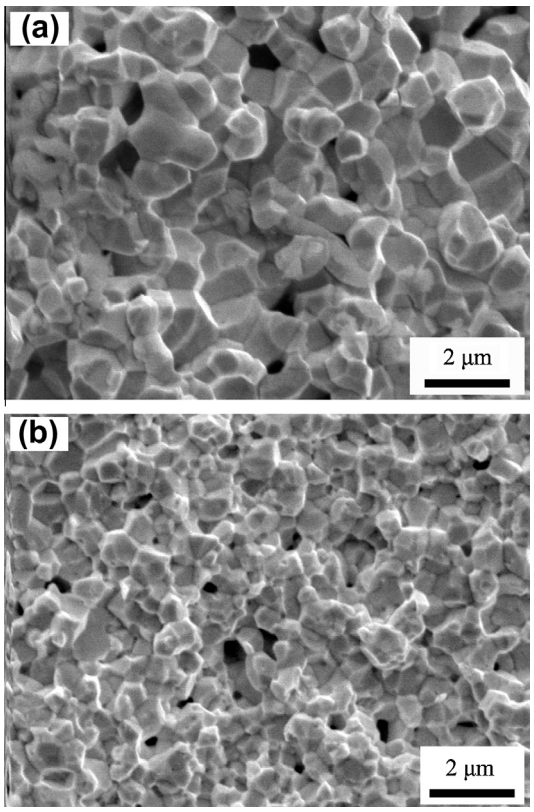

Fig. 4. SEM images of microwave-sintered (a) W–1%La_2O_3 and (b) W–1%Y_2O_3 from sol–gel produced powders.

Vickers micro-hardness of W–1%La_2O_3 and W–1%Y_2O_3 from sol–gel produced powders were measured as 4.12 and 6.03 GPa, respectively, as listed in Table 2. W–1%Y_2O_3 exhibits higher hardness than that of W–1%La_2O_3. The hardness is lower than those of ODS-W samples fabricated from ball-milled powders. This may be owing to the lower relative density of sol–gel synthesized ODS-W.

The fracture surfaces of microwave-sintered W–1%La_2O_3 and W–1%Y_2O_3 samples from sol–gel synthesized powders were presented in Fig. 4. The fresh fracture surface was obtained by breaking the specimens at ambient temperature, and was directly characterized by SEM without polishing or etching. It can be seen that the grain sizes of microwave-sintered ODS-W samples have grown to micron-scale, which are much larger than those of initial nano-sized powders (Fig. 3a and c). W–1%Y_2O_3 exhibited lower porosity, smaller pore size, and much smaller grains as compared to W–1%La_2O_3.

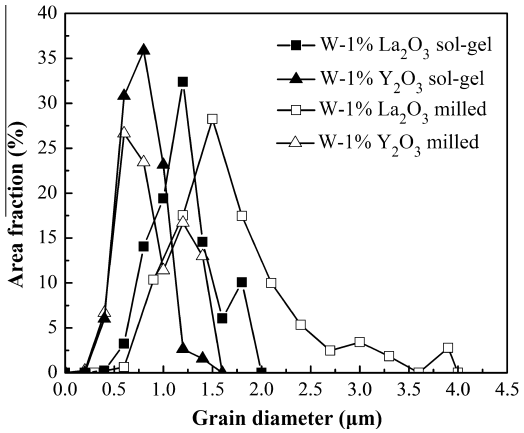

Fig. 5. Grain size distribution of microwave-sintered W–1%La_2O_3 and W–1%Y_2O_3 from sol–gel synthesized powders, where the results from the ball-milled powders were plotted for comparison.

The grain size distribution of ODS-W samples from sol–gel prepared powders was determined from the SEM micrographs, and shown in Fig. 5. Besides, the grain size distribution of microwave-sintered ODS-W from ball-milled commercial powders was also presented for comparison in Fig. 5. The grain size distribution of W–1%La_2O_3 is in the range from 0.3 to 2.0 μm, while that of W–1%Y_2O_3 is relatively narrow, in the range from 0.3 to 1.5 μm. The average grain size of W–1%La_2O_3 and W–1%Y_2O_3 is 1.1 μm and 0.7 μm, respectively. The results demonstrate that Y_2O_3 has better grain refinement effect on tungsten than La_2O_3.

As shown in Fig. 5, the grain size distribution of W–1%La_2O_3 from ball-milled commercial powders is in the range 0.3–4.0 μm with an average grain size of 1.4 μm. Sol–gel produced W–1%La_2O_3 shows much narrower grain size distribution and finer average grain size. Nevertheless, W–1%Y_2O_3 by sol–gel method and ball-milling method show similar grain size distribution and average grain size. For both sol–gel method and ball-milling method, W–1%Y_2O_3 samples show finer and more uniform grain size than W–1%La_2O_3 samples.

Yar et al. fabricated W–Y_2O_3 and W–La_2O_3 samples from chemically synthesized nano-powders by using spark plasma sintering method [18,19]. They reported that the average grain size of the W–1%Y_2O_3 sintered at 1200 °C and the W–0.9%La_2O_3 sintered at 1300 °C is about 2.3 and 4.2 μm, respectively, and the corresponding relative density is 92% and 88%. However, in the present work, much smaller grain size (0.7 and 1.1 μm) and higher relative density (93.8% and 92.4%) were obtained for W–1%Y_2O_3 and W–1%La_2O_3 even though they were microwave-sintered at 1500 °C.

TEM images of microwave-sintered W–1%Y_2O_3 from sol–gel produced tungsten powders were presented in Fig. 6. It can be seen

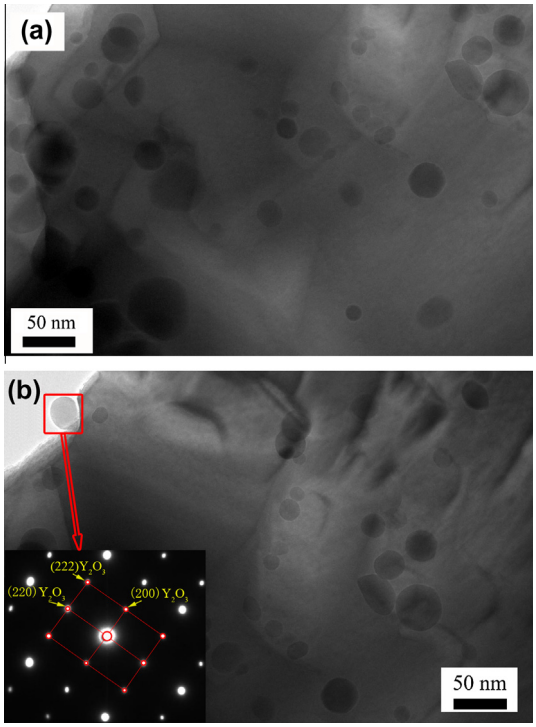

Fig. 6. TEM images (a and b) of microwave-sintered W–1%Y_2O_3 sample, and selected area diffraction pattern (inset in Fig. 6b) from a dispersoid particle at a grain boundary.

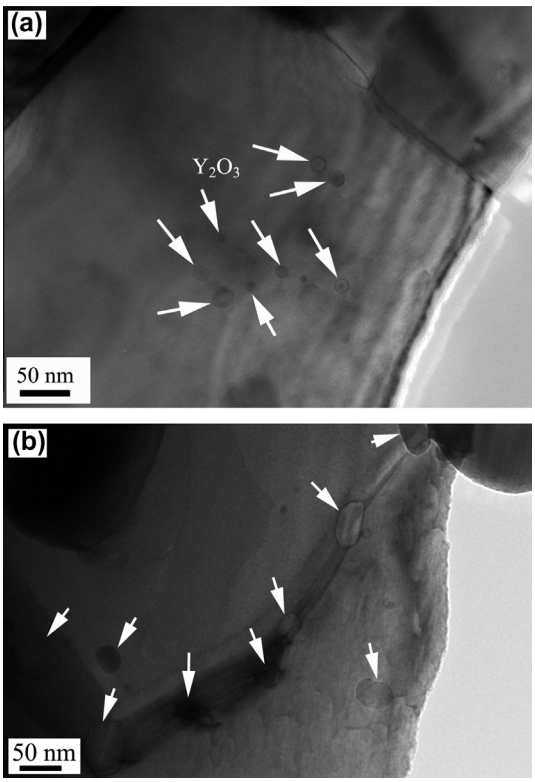

Fig. 7. TEM images showing the distribution of oxide particles in microwave-sintered W–1%Y_2O_3 from ball-milled commercial tungsten powders: (a) in the interior of a grain; and (b) on a grain boundary.

that many near-spherical oxide particles were homogeneously dispersed in the tungsten grains and on the grain boundaries, forming nano-structured materials. Most of the oxide particles is smaller than 50 nm. The inset to Fig. 6b showed the selected area electron diffraction pattern from a dispersoid particle at a grain boundary. It can be confirmed that the dispersoid is cubic Y_2O_3 phase. In our previous work, the fine-grained ODS-W samples were microwave-sintered from ball-milled commercial nano-sized tungsten and oxides powders [29]. The TEM micrographs of W–1%Y_2O_3 produced by ball-milled method were also presented in Fig. 7 for comparison. It can be seen that oxide particles with a size of 10–50 nm were dispersed in the tungsten grains and on the grain boundaries. The size of oxide particles is close to that of sol–gel produced W–1%Y_2O_3. However, the distribution of oxides particles is less homogeneous as compared to W–1%Y_2O_3 produced by sol–gel method (Fig. 6), in the aspect that the particle density of oxides is much higher in some area than elsewhere in the case of ball milling. The result shows the advantages of sol–gel method for fabricating nano-structured ODS-W with high homogeneity.

The homogeneous dispersion of oxide nano-particles in tungsten could pin dislocations and grains boundaries, and thus inhibit the grain growth, enhance the high temperature strength, and improve the recrystallization temperature. In addition, the dispersion of nano-sized oxide particles in tungsten matrix provides a large amount of interfaces. It is considered that the improvements in irradiation resistance of nano-materials relates to the high volume fraction of interfacial regions [12]. This kind of nano-structured materials should present good irradiation resistance because the large volume fraction of interfacial regions can serve as effective sinks for irradiation-induced point defects. On one hand, nano-sized oxide particles have grain-refinement effect on tungsten, which increase the volume fraction of the grain boundaries. On the other hand, the nano-sized oxide particles themselves increase the oxide/tungsten interfaces. Both aspects are beneficial to the improvement of irradiation resistance. The irradiation resistance ability of these nano-oxides dispersion strengthened tungsten materials would be studied in the near future.

4. Conclusions

Nano-sized W–1%La_2O_3 and W–1%Y_2O_3 powders were synthesized by sol–gel method followed by hydrogen reduction. The average particle sizes of tungsten is less than 50 nm. Microwave sintering method was used for the consolidation of tungsten samples, and a relatively low sintering temperature (1500 °C) and short soaking time (30 min) were used to inhibit the grain growth. The average grain size, and micro-hardness of the microwave-sintered W–1%La_2O_3 and W–1%Y_2O_3 samples are 1.1 μm and 0.7 μm, 4.12 and 6.03 GPa, respectively. In all, W–1%Y_2O_3 samples showed better sinterability, finer grains, and higher hardness as compared to W–1%La_2O_3 samples.

TEM characterization of W–1%Y_2O_3 showed that nano-sized oxide particles with a size distribution of 10–50 nm were homogeneously dispersed in tungsten matrix. The oxide particles distribution of ODS-W produced by sol–gel method is much more homogeneous than that produced by ball-milling method. The dispersion of oxide nano-particles in tungsten could not only improve the mechanical properties, but also provide a large amount of interfacial regions, which may act as sinks for irradiation-induced point defects and improve the irradiation resistance. Therefore, nano-oxides dispersion strengthened tungsten from sol–gel synthesized powders shows a possible access to high performance tungsten based materials, which was deserved for further investigation.

Acknowledgements

This work was financially supported by the Innovation Program (Grant No. KJCX2-YW-N35) and Strategic Priority Research Program (Grant No. XDA03010303) of Chinese Academy of Sciences, by the National Magnetic Confinement Fusion Program (Grant No. 2011GB108004), and by the National Natural Science Foundation of China (Grant Nos. 11075177, 91026002, 91126002, 11175203 and 51101152).

References

[1] I. Smid, H.D. Pacher, G. Vieider, U. Mszanowski, Y. Igitkhanov, G. Janeschitz, J. Schlosser, L. Plochl, J. Nucl. Mater. 233–237 (1996) 701–707.
[2] T. Hino, M. Akiba, Fusion Eng. Des. 49–50 (2000) 97–105.
[3] P. Norajitra, L.V. Boccaccini, E. Diegele, V. Filatov, A. Gervash, R. Giniyatulin, S. Gordeev, V. Heinzel, G. Janeschitz, J. Konys, W. Krauss, R. Kruessmann, S. Malang, I. Mazul, A. Moeslang, C. Petersen, G. Reimann, M. Rieth, G. Rizzi, M. Rumyantsev, R. Ruprecht, V. Slobodtchouk, J. Nucl. Mater. 329–333 (2004) 1594–1598.
[4] E. Diegele, R. Krussmann, S. Malang, P. Norajitra, G. Rizzi, Fusion Eng. Des. 66–68 (2003) 383–387.
[5] P. Norajitra, L.V. Boccaccini, A. Gervash, R. Giniyatulin, N. Holstein, T. Ihli, G. Janeschitz, W. Krauss, R. Kruessmann, V. Kuznetsov, A. Makhankov, I. Mazul, A. Moeslang, I. Ovchinnikov, M. Rieth, B. Zeep, J. Nucl. Mater. 367–370 (2007) 1416–1421.
[6] H. Kurishita, S. Kobayashi, K. Nakai, T. Ogawa, A. Hasegawa, K. Abe, H. Arakawa, S. Matsuo, T. Takida, K. Takebe, M. Kawai, N. Yoshida, J. Nucl. Mater. 377 (2008) 34–40.
[7] H. Kurishita, Y. Amano, S. Kobayashi, K. Nakai, H. Arakawa, Y. Hiraoka, T. Takida, K. Takebe, H. Matsui, J. Nucl. Mater. 367–370 (2007) 1453.
[8] Y. Zhang, A.V. Ganeev, J.T. Wang, J.Q. Liu, I.V. Alexandrov, Mater. Sci. Eng., A 503 (2009) 37–40.
[9] Y. Ishijima, H. Kurishita, K. Yubuta, H. Arakawa, M. Hasegawa, Y. Hiraoka, T. Takida, K. Takebe, J. Nucl. Mater. 329–333 (2004) 775–779.
[10] G. Ackland, Science 327 (2010) 1587–1588.
[11] H. Kurishita, T. Kuwabara, M. Hasegawa, S. Kobayashi, K. Nakai, J. Nucl. Mater. 343 (2005) 318–324.
[12] N. Nita, R. Schaeublin, M. Victoria, J. Nucl. Mater. 329–333 (2004) 953–957.

[13] M. Samaras, P.M. Derlet, H.V. Swygenhoven, M. Victoria, Phys. Rev. Lett. 88 (2002) 12.
[14] X.M. Bai, A.F. Voter, R.G. Hoagland, M. Nastasi, B.P. Uberuaga, Science 327 (2010) 1631–1634.
[15] T. Chookajorn, H.A. Murdoch, C.A. Schuh, Science 337 (2012) 951–954.
[16] Y. Kim, K.H. Lee, E.-P. Kim, D.-I. Cheong, S.H. Hong, Int. J. Refract. Met. Hard Mater. 27 (2009) 842–846.
[17] M. Rieth, B. Dafferner, J. Nucl. Mater. 342 (2005) 20–25.
[18] M.A. Yar, S. Wahlberg, H. Bergqvist, H.G. Salem, M. Johnsson, M. Muhammeda, J. Nucl. Mater. 408 (2011) 129–135.
[19] M.A. Yar, S. Wahlberg, H. Bergqvist, H.G. Salem, M. Johnsson, M. Muhammeda, J. Nucl. Mater. 412 (2011) 227–232.
[20] A. Muñoz, M.A. Monge, B. Savoini, M.E. Rabanal, G. Garces, R. Pareja, J. Nucl. Mater. 417 (2011) 508–511.
[21] I. Wesemann, W. Spielmann, P. Heel, A. Hoffmann, Int. J. Refract. Met. Hard Mater. 28 (2010) 687–691.
[22] Y. Kim, M.-H. Hong, S.H. Lee, E.-P. Kim, S. Lee, J.-W. Noh, Met. Mater. Int. 12 (3) (2006) 245–248.
[23] M.V. Aguirre, A. Martín, J.Y. Pastor, J. LLorca, M.A. Monge, R. Pareja, J. Nucl. Mater. 404 (2010) 203–209.
[24] R. Roy, D. Agrawal, J. Cheng, S. Gedevanishvili, Nature 399 (1999) 668–670.
[25] K. Saitou, Scripta Mater. 54 (2006) 875–879.
[26] J. Cheng, D. Agrawal, Y. Zhang, R. Roy, Mater. Lett. 56 (2002) 587–592.
[27] S. Wurster, R. Pippan, Scripta Mater. 60 (2009) 1083–1087.
[28] G. Prabhu, A. Chakraborty, B. Sarma, Int. J. Refract. Met. Hard Mater. 27 (2009) 545–548.
[29] R. Liu, Y. Zhou, T. Hao, T. Zhang, X.P. Wang, C.S. Liu, Q.F. Fang, J. Nucl. Mater. 424 (2012) 171–175.